ACS Energy Letters

http://pubs.acs.org/journal/aelccp

Harvesting Ocean Wave Energy via Magnetoelastic Generators for Self-Powered Hydrogen Production

Il Woo Ock,[†] Yihao Zhou,[†] Xun Zhao, Farid Manshaii, and Jun Chen*

Cite This: *ACS Energy Lett.* 2024, 9, 1701−1709

Read Online

ABSTRACT: **Extracting energy from ocean waves for electrolysis, while highly desirable, poses significant challenges, especially in achieving high current generation for sustainable water splitting. This work introduces an innovative high-current ocean wave energy harvesting system, employing a self-floating magnetoelastic generator (MEG) ball network designed for autonomous seawater electrolysis and *on-site* hydrogen (H_2) production. Leveraging the magnetoelastic effect, the MEG ball network is naturally waterproof and can generate a high current density of 0.24 mA cm^{-2}, paired with a low internal resistance of 9 Ω at a wave frequency of 2 Hz. Its spherical design ensures exceptional mechanical durability, maintaining consistent electrical output even under extremely humid and harsh conditions. In practical applications, this MEG ball network system can continuously produce H_2 at a rate of 0.76×10^{-3} mL min^{-1}. These results underscore its potential as a viable technology for *on-site* seawater electrolysis and large-scale H_2 production.**

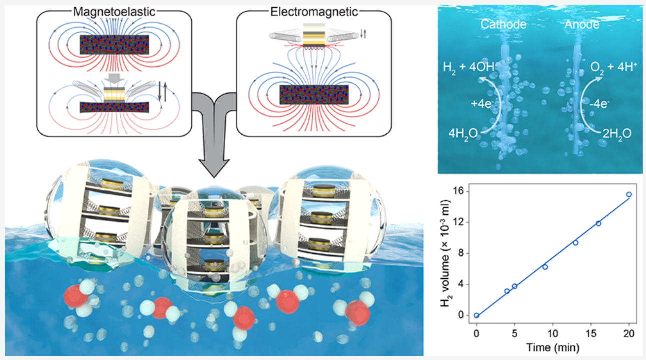

Ocean wave energy, an abundant and sustainable energy source, demonstrates greater resilience to ambient conditions compared to other renewable energies such as wind and solar. It remains consistently available regardless of season, time of day, weather, or temperature variations.[1−4] Approximately 71% of the Earth is covered by oceans, with ocean waves having the potential to generate 8000 to 80 000 terawatt-hours of electrical energy annually.[5,6] Despite this substantial potential, wave energy utilization in the overall world energy consumption is still largely underexplored.

Currently, the dominant method for harnessing mechanical kinetic energy from ocean waves centers around electromagnetic generators (EMGs).[7−11] However, there are significant challenges in deploying EMGs for ocean wave energy harvesting. First, due to the use of magnets and metal coils, the inherent weight and mass density of EMGs impede their ability to float naturally, necessitating additional support structures such as floaters or buoy platforms. Second, EMGs are optimized for capturing energy from flowing streams, which may not be as efficient for harnessing wave energy in various directions. Lastly, their need for high-quality materials could make EMGs cost-inefficient for large-scale applications.[12,13] Moreover, ocean waves are typically irregular in frequency and amplitude, leading to unstable electrical outputs. Efficiently transmitting these electrical signals from the ocean to land poses another grand challenge.[14,15]

A more desirable and efficient alternative could be to convert ocean wave energy directly into electricity and store it as chemical fuels.[16,17] Compared to electrical power transmission and electrochemical energy storage, chemical fuels offer higher stability, ease of storage, and transportability. In this context, seawater electrolysis powered by renewable energy sources has emerged as a sustainable method for producing green hydrogen (H_2).[18−25] However, practical feasibility is hindered by low current generation and instability against ambient humidity.

To overcome these challenges, we introduce a self-floating magnetoelastic generator (MEG) ball network as a novel, inherently waterproof platform technology for water wave energy harvesting. The working mechanism of the MEG relies

Received: February 8, 2024
Revised: March 10, 2024
Accepted: March 19, 2024
Published: March 25, 2024

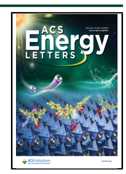

https://doi.org/10.1021/acsenergylett.4c00412
ACS Energy Lett. 2024, 9, 1701−1709

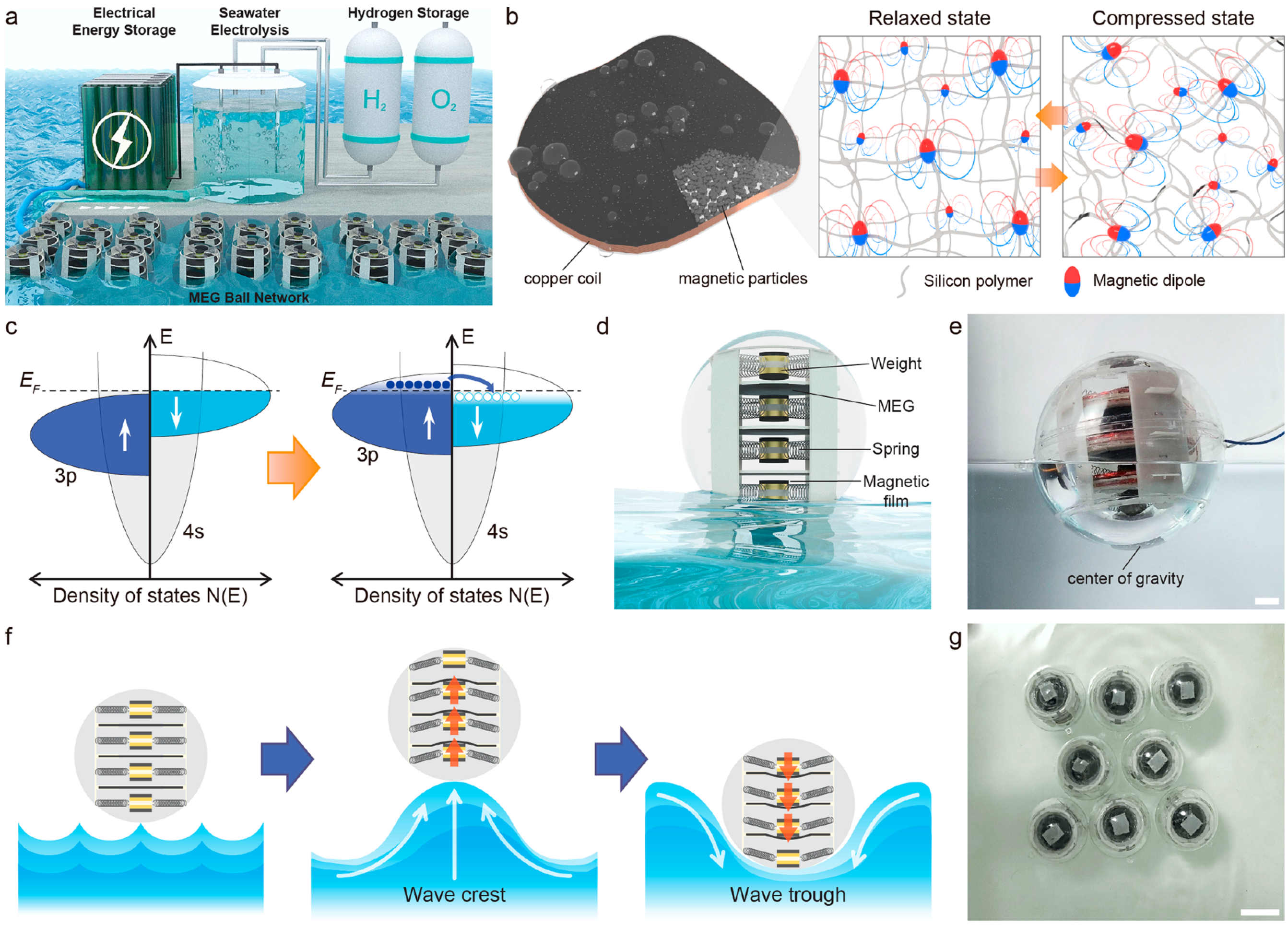

Figure 1. Energy harvesting from ocean waves via the MEG ball network for self-powered hydrogen production. (a) Schematic showing the design of the self-powered seawater-splitting system, including the MEG ball network, electrical energy storage, seawater electrolysis, and hydrogen storage, converting ocean wave energy to H_2 fuel. (b) Illustration of the wavy chain model of the MC layer, demonstrating giant magnetoelasticity. (c) Density of states in the MC layer before (left) and after (right) compression, illustrating the magnetoelastic effect. (d) Design structure of the self-floating MEG ball network for harvesting ocean wave energy. (e) Photograph of a fabricated MEG ball network floating on water. Scale bar: 1 cm. (f) Illustration of the MEG ball network's energy generation mechanism for a single ocean wave cycle. (g) Photograph of the MEG ball network on the water surface. Scale bar: 5 cm.

on the magnetoelastic effect, an effect recently discovered in soft materials systems in 2021.[26] The magnetoelastic effect involves changes in the magnetic flux density of materials when subjected to mechanical stress in the presence of an external magnetic field. This effect was first observed by the Italian experimental physicist Emilio Villari in 1865.[27] Known as the Villari effect, the magnetoelastic effect is the inverse magnetostrictive effect and has been identified in various rigid metals and metal alloys, such as $Fe_{1-x}Co_x$,[28] $Tb_xDy_{1-x}Fe_2$ (Terfenol-D),[29] and Ga_xFe_{1-x} (Galfenol).[30] Not until 2021 was the magnetoelastic effect discovered in a soft polymer system, which was coupled with magnetic induction to develop a MEG as a new working mechanism to revive mechanical energy conversion.[26] It features high current density, low inner impedance, and intrinsic waterproofness.[31−34] The MEG ball network is designed to convert ocean waves into high-current electrical signals for self-powered, eco-friendly H_2 production. Each MEG device, shaped like a ball, can generate a high current density of 0.24 mA cm^{-2} at an extremely low resistance of 9 Ω under a wave frequency of 2 Hz. A MEG ball network can be formed by scaling up these MEG balls and connecting them electrically. This network demonstrates a charging capability that can elevate the potential of a commercial capacitor to approximately 7 V in about 6 min. Additionally, the system is integrated into a seawater-splitting cell, enabling continuous generation of high-energy-density H_2 fuel at a rate of 0.76×10^{-3} mL per minute.

By bypassing reliance on the existing grid and directly leveraging abundant ocean energy, this approach minimizes long-distance current carrying and allows for the use of *on-site*-generated H_2 for heavy-duty transportation, such as in cargo ships or coastal refinery heavy oil upgrading, eliminating the need for extensive H_2 transportation. This strategy presents a promising pathway toward embracing ocean wave energy and utilizing it effectively in sustainable energy production and transportation, contributing significantly to reducing the energy crisis, achieving net zero emissions, and advancing carbon neutrality.

Ocean wave energy serves as an abundant and sustainable source of continuous kinetic energy, enabling seawater conversion into H_2 fuel through an energy conversion system. Figure 1a depicts our self-floating MEG ball network, which efficiently transforms ocean wave energy into a H_2-based blue energy fuel. Each MEG unit in the network is constructed from

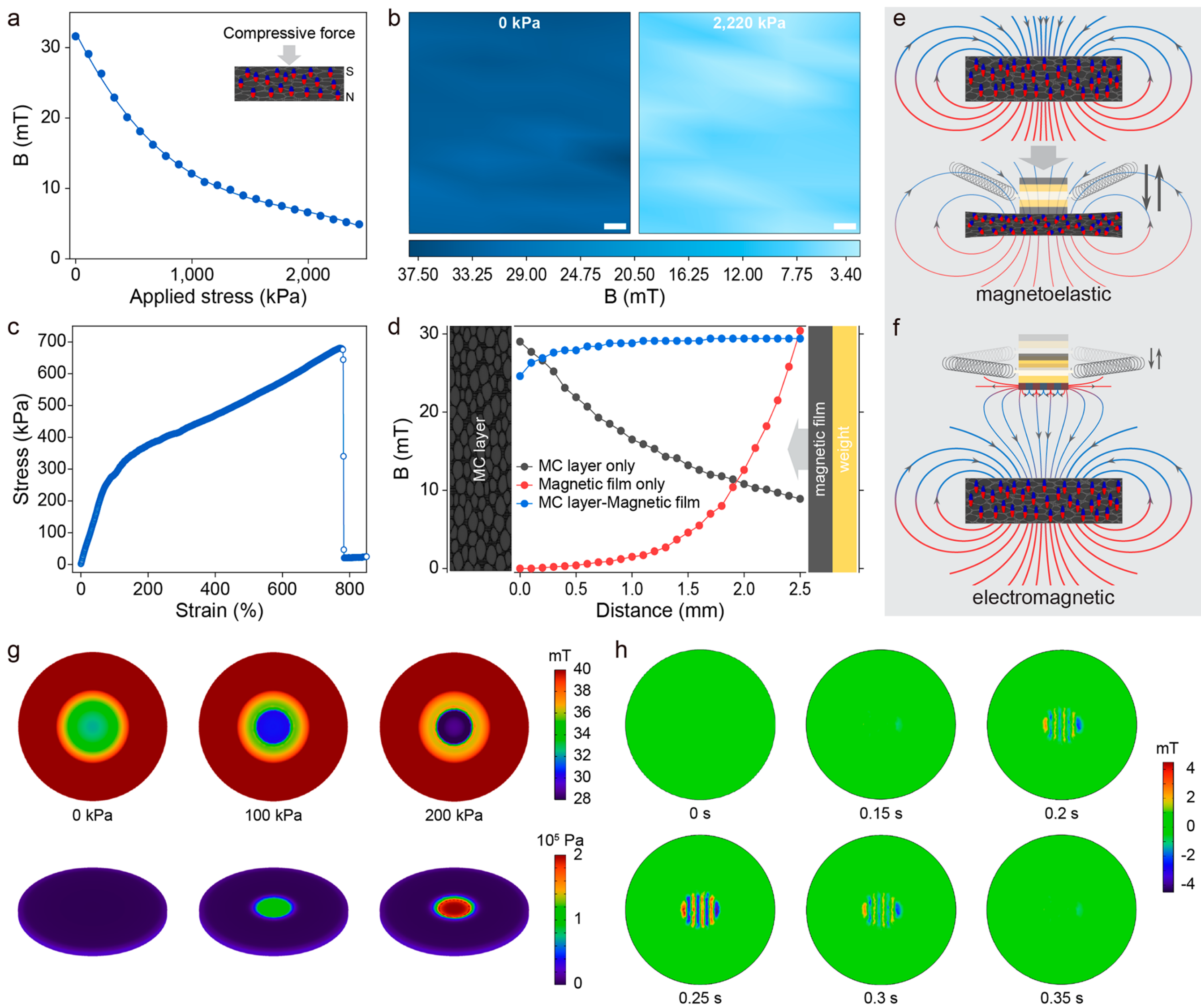

Figure 2. Working mechanism of a MEG unit in ocean wave energy conversion. (a) Magnetic field variation in the MC layer under compressive forces ranging from 0 to 2400 kPa. (b) 2D magnetic flux density mapping of the MC layer in its original state (0 kPa) and under compression (2220 kPa). Scale bar: 0.2 cm. (c) Stress−strain curve of the MC layer. (d) Variation in central surface magnetic field based on distance. (e) Illustration explaining the magnetoelastic effect in high-amplitude waves. (f) Illustration explaining the electromagnetic effect in low-amplitude waves. (g) Simulated magnetic flux density and pressure distributions in the MC layer under pressures of 0, 100, and 200 kPa. (h) Simulated magnetic flux density changes at the surface of the MC layer when the magnetic film approaches and recedes.

lightweight, mechanically durable, and chemically stable plastic materials, designed to float on water surfaces and harvest wave energy even in harsh oceanic environments. A MEG unit comprises two key components: the magnetomechanical coupling (MC) layer and the magnetic induction (MI) layer. The MC layer, consisting of magnetic particles and a silicon polymer, forms a wavy structure matrix that is intrinsically waterproof. The MI layer, embedded within the MC layer, includes a metal coil. When the MC layer deforms due to kinetic wave energy, the arrangement of magnetic particles changes, leading to variations in the magnetic properties of the MC layer, which is called the magnetic particle−particle interaction (MPPI) (Figure 1b). The magnetic flux density variation further influences the change in the electronic density of states within the micromagnets (Figure 1c). Micromagnetic particles, being strong ferromagnetic materials, become magnetized and exhibit an anisotropic band structure. External strains cause the majority spin band to increase in energy due to spin−orbital coupling, while the minority spin band decreases in energy due to structural changes.[35] This discrepancy in the electronic band for up and down spins is a result of the magnetic dipole−dipole interaction (MDDI), which alters the magnetic characteristics of the MC layer.

Collectively, MPPI and MDDI synergically affect the magnetic flux perceived by the MI layer, leading to electromotive force (EMF) generation as described by eq 1:

$$\varepsilon = -N\frac{d\Phi}{dt} \tag{1}$$

where ε represents the induced EMF, N is the turn count of the coil, Φ is the magnetic flux, and t denotes time. Further theoretical studies and investigations will delve into the physical origins of MEG to fully understand the giant magnetoelastic effects.

https://doi.org/10.1021/acsenergylett.4c00412
ACS Energy Lett. 2024, 9, 1701−1709

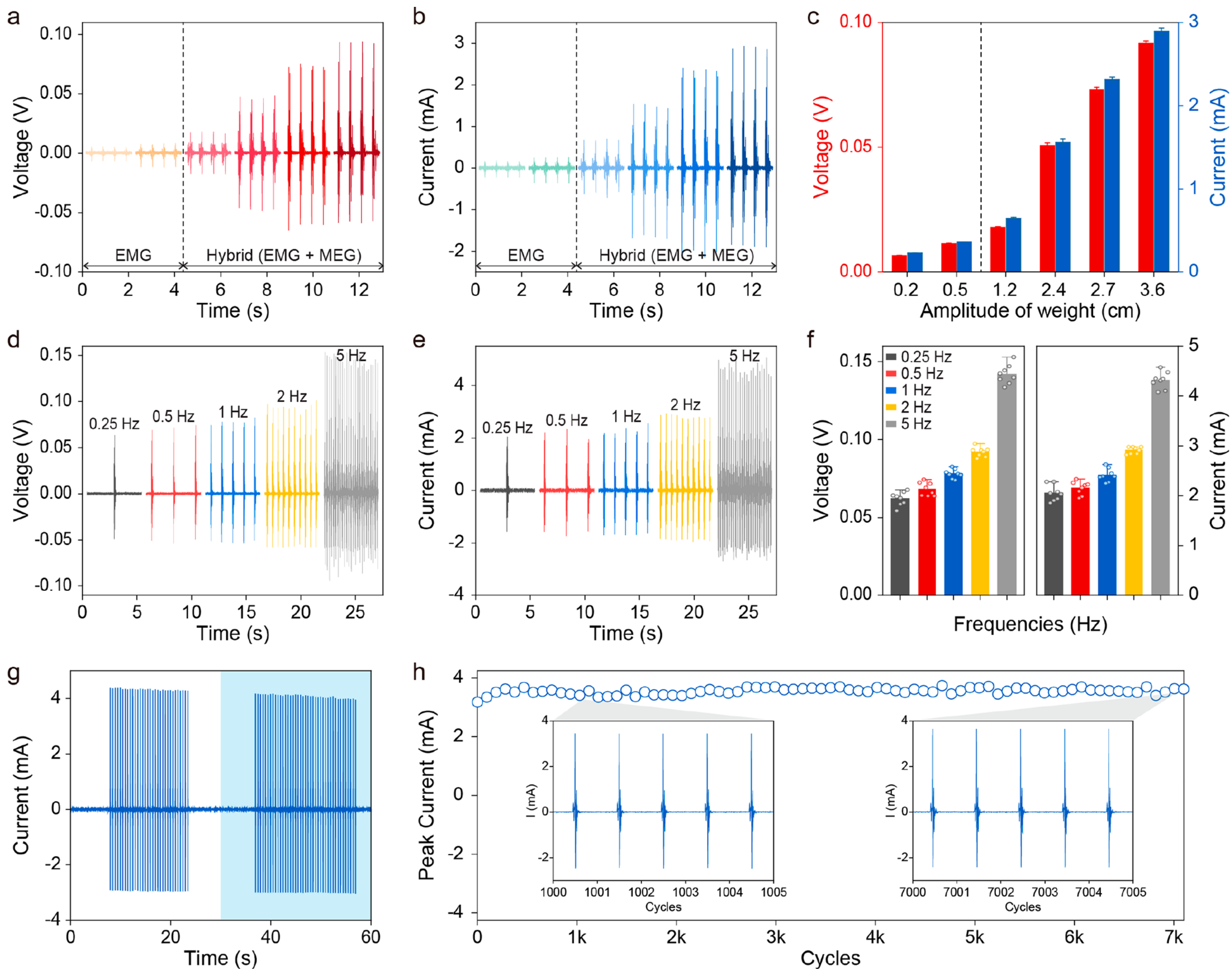

Figure 3. Output performance characterization of a MEG unit under different wave conditions. (a) V_{oc}, (b) I_{sc}, and (c) dependence of V_{oc} and I_{sc} on various wave energies. The error bars represent the standard deviation of the eight peak points of the measured data. (d) V_{oc}, (e) I_{sc}, and (f) dependence of V_{oc} and I_{sc} on different wave frequencies from 0.25 to 5 Hz. The error bars represent the standard deviation of the eight peak points of the measured data. (g) I_{sc} measurements before and after water exposure. (h) Cyclic testing of a MEG unit over 7000 cycles, with enlarged data from 1000 to 1005 cycles and 7000 to 7005 cycles.

Based on the working mechanism, the MEG ball network is engineered to float vertically relative to the water surface, enhancing the ocean wave energy conversion efficiency. The ball-shaped floating devices readily float on water without concerns about sinking and exhibit a symmetric shape that minimizes damage risk while enabling uniform energy conversion. This MEG ball network design, including an outer protective shell, is illustrated in Figure 1d. The network comprises three fixed MEG units and four spring-assisted weights, each fitted with a magnetic film. These components are arranged in a stacked formation, enabling the device to self-float owing to the weight affixed at the bottom of the MEG ball, thereby lowering its center of gravity (Figure 1e). Wave-induced weight movements cause sequential deformation of the MEG units throughout a wave cycle (Figure 1f). At this point, the weight is designed to be anchored in four directions with identical springs, allowing only vertical movement (Figure S1). Eight precisely engineered MEG ball networks are linked in series to boost the current output, serving as a sustainable power source for H_2 fuel production. This configuration creates a high aspect ratio network on the water surface, thereby increasing the power output (Figure 1g).

To comprehend the power generation capabilities of the MEG ball network, we assessed the magnetic and mechanical properties of the MC layer. Subjected to external kinetic forces, the MC layer shows variations in surface magnetic flux density. Figure 2a displays these variations in response to compressive forces ranging from 0 to 2400 kPa. The magnetic flux density of the MC layer experiences an exponential decrease of approximately 85%, falling from 31.6 mT (0 kPa) to 4.9 mT (2400 kPa), with a maximum magnetomechanical coupling factor of 2.41×10^{-8} T Pa^{-1}. The decrease in magnetic flux density is attributed to MPPI and MDDI, resulting from changes in magnetic dipoles and the interdistance between magnetic particles when vertical pressure is applied (Figure S2). The magnetic changes of the MC layer are further evident in the 2D magnetic flux mapping. A scanning electron microscope (SEM) image (Figure S3) shows a uniform, dense distribution of magnetic particles in a wavy chain structure corresponding to the initial magnetic flux density state (Figure 2b). At 0 kPa, the magnetic flux remains

https://doi.org/10.1021/acsenergylett.4c00412
ACS Energy Lett. 2024, 9, 1701−1709

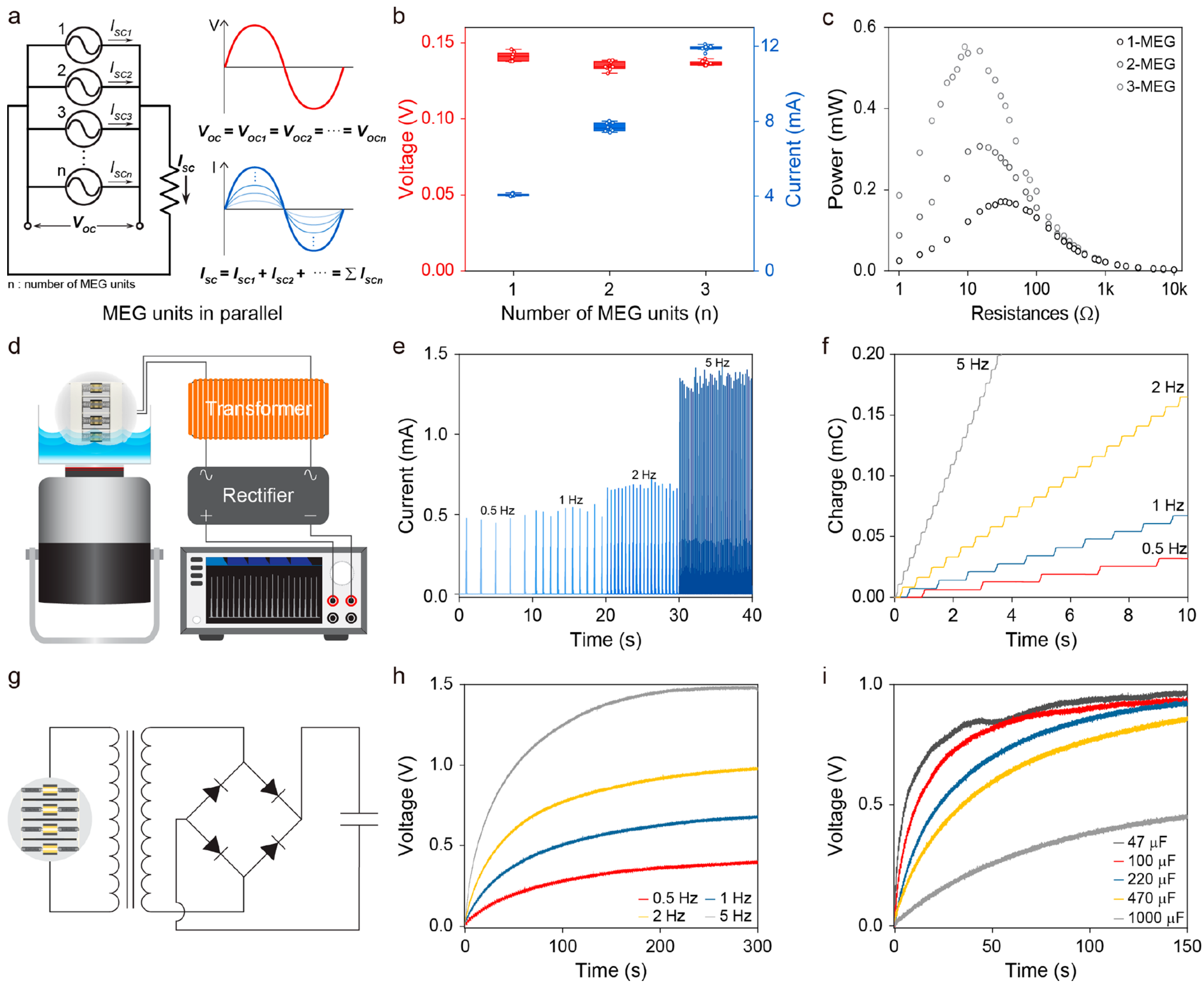

Figure 4. Performance output characterization of MEG ball networks. (a) Circuit diagram of MEG units connected in parallel within a network. (b) Dependence of V_{oc} and I_{sc} on the number of parallel-connected MEG units. The error bars represent the standard deviation of the eight peak points of the measured data. (c) Calculated output power corresponding to V_{oc} and I_{sc} with varying numbers of MEG units. (d) Illustration of the power management circuit setup for a wave energy harvesting system. (e) Transformed and rectified output current and (f) transferred charge on different wave frequencies from 0.5 to 5 Hz. (g) Circuit diagram for charging a commercial capacitor using the MEG ball network. (h) Voltage increases in the commercial capacitor at different wave frequencies from 0.5 to 5 Hz. (i) Charging characteristics of commercial capacitors with varying capacitance at a 2 Hz wave frequency.

consistent between 28 to 33 mT. However, at a vertical pressure of 2220 kPa, a significant reduction is shown in intensity, dropping to a maximum of 3.4 mT. It is crucial to quantify a device's deformation accurately under external conditions. The stress−strain curve of the MC layer, depicted in Figure 2c, demonstrates its impressive elastic stretchability, with up to 781% deformation and a relatively low Young's modulus of 680.4 kPa. This highlights the durability of the MEG device in maintaining efficient operation for wave energy harvesting.

The MEG device exhibits variations in its magnetic characteristics when subjected to deformation within the MC layer or when the magnetic film approaches the proximity of the MC layer. The alteration in magnetic flux density on the central surface of the MC layer, concerning different distances, was measured in response to changes in external magnetic fields (Figures 2d and S4). As the distance between the MC layer and the magnetic film increases, both components experience a decrease in magnetic flux, particularly the magnetic film, which saturates from 30 to 0 mT when the distance reaches 2.5 mm. Conversely, when the MC layer and the magnetic film come closer, the magnetic field initially reduces slightly, followed by a substantial decrease starting at approximately 1 mm (Figure S4c). Magnetic films exhibit alternative dipole distributions, resulting in minimal variations even with reduced distances from the MC layer, showing the significant changes occurring only at the center. These observations of magnetic field variation help elucidate the operational mechanism of the MEG ball network, confirming the combined influence of magnetoelastic and electromagnetic effects on the energy transmitted through wave energy (Figure 2e,f). To investigate the magnetoelastic and electromagnetic effects in the MEG unit, we used COMSOL Multiphysics software to simulate the magnetic flux density of the MC layer.

https://doi.org/10.1021/acsenergylett.4c00412
ACS Energy Lett. 2024, 9, 1701−1709

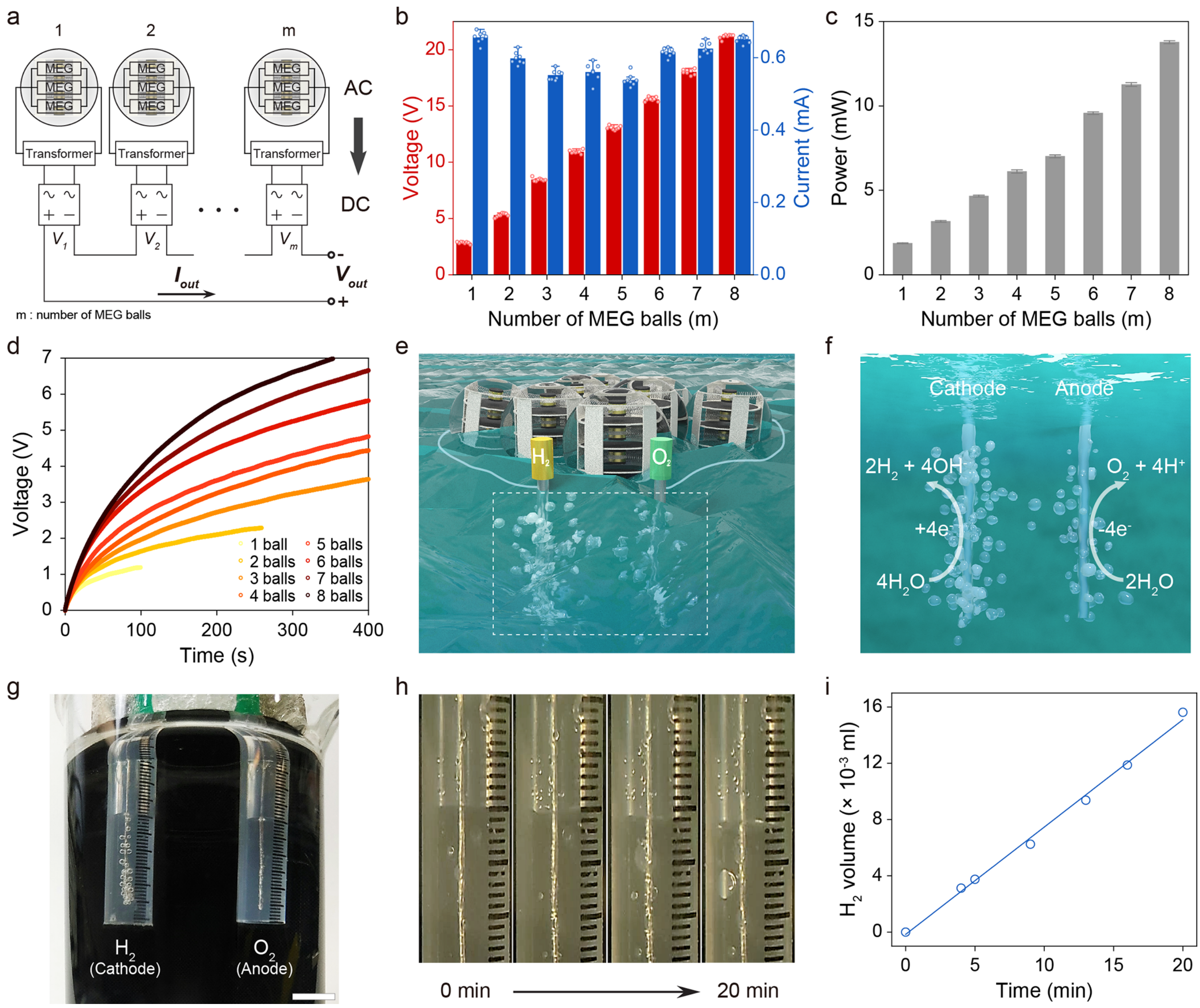

Figure 5. Self-powered seawater-splitting system powered by the MEG ball network. (a) Schematic diagram of the MEG ball network with MEG balls connected in series for wave energy harvesting. (b) Dependence of V_{oc} and I_{sc} on the number of MEG balls. The error bars represent the standard deviation of the eight peak points of the measured data. (c) Calculated peak power of the MEG ball network corresponding to V_{oc} and I_{sc}. (d) Voltage curves of a commercial capacitor charged by the MEG ball network with varying numbers of MEG balls (from 1 to 8). (e) Illustration of the self-powered seawater-splitting system driven by the MEG ball network. (f) Schematic representation of seawater-splitting in a two-electrode system. (g) Optical image of Pt(C)/Pt(A) two-electrode seawater-splitting in a 3.5 wt % NaCl aqueous solution. Scale bar: 5 cm. (h) Optical images showing H_2 collection in a syringe over 20 min. (i) Graph depicting H_2 production volume as a function of time.

Figure 2g shows the magnetic flux distribution when mechanical stresses of 0, 100, and 200 kPa are applied to the MC layer by moving the magnetic film vertically. The simulation results, which align with experimental data, show a notable decrease in intensity (Figure S5), elucidating the giant magnetoelastic effect. Additionally, we simulated the magnetic flux variation on the surface of the MC layer when the magnetic film oscillates without deforming the MC layer (Figure 2h). The magnetic film, displaying a periodic arrangement of the north and south poles, yields an intensity value of about 30 mT (Figure S6). As the magnetic film approaches the MC layer, changes in the surface magnetic flux distribution occur, demonstrating an electromagnetic effect with intensity variations around 4 mT. Therefore, the MEG ball network can operate in both contact and noncontact modes due to the magnetic film's movement. The simultaneous magnetoelastic and electromagnetic effects lead to electricity generation, facilitating energy conversion.

Understanding the performance of the MEG ball network in relation to various wave energies is crucial. Optimal electrical outputs under different conditions were measured, including the open-circuit voltage (V_{oc}) and short-circuit current (I_{sc}) for different wave energies (Figure 3a−c and Table S1). For wave energies up to a 0.5 cm amplitude, noncontact electromagnetic interaction resulted in a maximum output of 11.3 mV and 0.36 mA, while contact-induced hybrid interaction yielded 91.6 mV and 2.98 mA for amplitudes exceeding 1.2 cm. Moreover, the MEG unit showed increasing electrical output trends with an amplitude of 3.6 cm at frequencies from 0.25 to 5 Hz (Figure 3d−f and Table S2). Notably, at 5 Hz, the MEG unit achieved a peak output with V_{oc} of 142.3 mV and I_{sc} of 4.31 mA. These

https://doi.org/10.1021/acsenergylett.4c00412
ACS Energy Lett. 2024, 9, 1701−1709

results demonstrate the effectiveness of MEG devices in wave energy conversion, even in harsh ocean environments.

The capability of the MEG ball network to generate electricity sustainably from wave energy on the water surface is further strengthened by its intrinsic waterproofness. Figure 3g shows that the generated current remains stable when exposed to water. Even after being soaked in salty water (3.5 wt % NaCl aqueous solution) similar to seawater for 24 h, the MEG unit maintains its initial output performance, affirming its intrinsic waterproofness (Figure S7). The device also exhibited stable electrical output over 7000 mechanical cycles (Figure 3h), with the current generation maintaining a consistent waveform over time, highlighting the MEG's durability.

Next, we optimized the output performance of the MEG ball network for ocean wave energy harvesting. All MEG units are composed of a magnetized MC layer in the same direction and copper coils with identical structures, which help to prevent electrical output cancellation (Figures 4a and S8). Three MEG units connected in parallel formed the MEG ball network, and the output performance was measured based on the number of MEG units. According to Ohm's law, the parallel-connected MEGs maintained V_{oc} values from 135 to 142 mV, while the I_{sc} increased linearly with more MEG units. For example, with one, two, and three units connected in parallel, I_{sc} values were 4.06, 7.68, and 11.91 mA, respectively (Figures 4b and S9 and Table S3). The output powers with different numbers of units were compared, and V_{oc} and I_{sc} were measured under various resistive loads from 1 to 10 000 Ω. The peak power increased linearly from 0.17, 0.31, and 0.55 mW with more MEG units but showed an opposite trend in I_{sc}, where resistance decreased to 35, 15, and 9 Ω as the number of units increased (Figures 4c and S10). The electrical output with MEG units connected in series was also measured (Figures S11−S13 and Table S4). As the number of MEG units increased, V_{oc} linearly increased to 142.1, 287.2, and 407.0 mV, while I_{sc} remained between 4.06 and 4.21 mA. The calculated power output increased to 0.17, 0.29, and 0.50 mW, according to V_{oc}. However, the resistance increased up to 100 Ω when using three MEG units in series. For efficient energy harvesting, the MEG ball network should have a low inner impedance to maximize energy conversion and minimize electrical loss. Thus, the parallel connection of MEG units is more effective, increasing the total current density and charge transfer per unit of time.

The ocean wave energy harvesting system was emulated by using a shaker to generate mechanical vibration. The alternating current (AC) output from each MEG ball network was transformed and rectified into direct current (DC) power through a management circuit (Figure 4d). The transformed voltage increased to 2.22 V with a current of 0.66 mA, yielding an efficiency of approximately 90% (Figure S14). The transformed and rectified output characteristics at different water wave frequencies from 0.5 to 5 Hz were measured (Figures 4e and S15), showing increased peak current and voltage values at higher frequencies. At 5 Hz, peak values reached 1.32 mA and 4.14 V, respectively. Within a single cycle, transferred charges of 5.94, 6.87, 8.27, and 10.78 μC were achieved for waves with frequencies of 0.5, 1, 2, and 5 Hz (Figure 4f). The transferred charge of a MEG ball network reached 0.2 mC within 3.6 s at 5 Hz. Commercial capacitors charged under different wave conditions demonstrated the MEG's charging capability, with voltage saturation achieved within 300 s at various frequencies (Figure 4g). In Figure 4h, the voltage initially increased rapidly and then saturated to a constant value. For instance, at frequencies of 0.5, 1, 2, and 5 Hz, the saturated voltage values were 0.39, 0.68, 0.97, and 1.48 V within 300 s. Furthermore, capacitors with larger capacitances require more time to reach the same charging voltage, and the voltage across the capacitor saturates exponentially over time after passing through the initial linear charging phase (Figures 4i and S16 and Table S5). The charging of a capacitor utilizing the MEG ball network can be observed to follow the equation as follows:

$$V = \frac{Q}{C} \tag{2}$$

$$V(t) = V_0(1 - e^{-t/RC}) \tag{3}$$

where V represents capacitor voltage, V_0 is the external voltage, Q is charge, R is resistance, C is capacitance, and t denotes time. On the contrary, comparing the series connection of three MEG units reveals a trade-off between voltage and current due to the increased internal resistance. While different output values result in a higher potential for the charged capacitor, a lower output current extends the time to reach saturation as the capacitance increases (Figures S17 and S18).

MEG balls were connected in series to form a network for water wave energy harvesting, as shown in Figure 5a. Each network included a transformer and a bridge rectifier to increase the output voltage. The network, comprising one to eight interconnected MEG balls, demonstrated a linear increase in V_{oc} to a maximum of 21.17 V with eight MEG balls, while the output current ranged from 0.60 to 0.66 mA (Figures 5b and S19, and Table S6). Each MEG ball network provided about 1.87 mW, with a maximum output of around 13.78 mW for an eight-MEG configuration (Figure 5c). The network also showed fast voltage charging characteristics, raising the voltage of a commercial capacitor to 7 V within 350 s (Figure 5d).

The MEG ball network is linked to a self-powered electrochemical energy conversion system driven by wave energy serving as the primary power source (Figure 5e). This system, employing a Pt(cathode)/Pt(anode) symmetric cell, facilitates seawater-splitting, producing hydrogen (H_2) at the cathode and oxygen (O_2) at the anode, driven by the potential applied to both electrodes (Figure 5f). The chemical reactions are as follows:[36]

$$2H_2O \rightarrow 2H_2 + O_2 \text{ (Overall)} \tag{4}$$

$$4H^+ + 4e^- \rightarrow 2H_2 \text{ (Cathode)} \tag{5}$$

$$2H_2O \rightarrow O_2 + 4H^+ + 4e^- \text{ (Anode)} \tag{6}$$

Electrochemical water-splitting theoretically requires a voltage of 1.23 V.[37] However, the complexity of the oxygen evolution reaction (OER) raises the threshold overpotential for water decomposition, especially in seawater. Challenges include high-energy barriers from the chlorine evolution reaction (ClER) at the anode, reduced electrolysis efficiency due to suspended particles, and seawater's low conductivity.[38] To determine the onset voltage of our seawater-splitting system, we measured the linear sweep voltammetry (LSV) curve at a scan rate of 10 mV s^{-1} in a 3.5 wt % NaCl aqueous solution. The current sharply increased after approximately 2.4 V (Figure S20). This confirms that the onset voltage of the MEG ball network is

https://doi.org/10.1021/acsenergylett.4c00412
ACS Energy Lett. 2024, 9, 1701−1709

sufficient for directly driving seawater-splitting, as H_2 and O_2 are produced at the cathode and anode, respectively.

We also measured the H_2 fuel generated by the MEG ball network. A Pt rod was positioned upside down inside a syringe with one side open to seawater. Both the cathode and anode were connected to the MEG ball network (Figure 5g). The produced H_2 gas accumulated inside the syringe, and its volume was calculated based on water level changes over time. Figure 5h displays the variation in accumulated H_2 during 20 min of operation, and the corresponding data is presented in Figure 5i. The H_2 production rate was 0.76×10^{-3} mL min^{-1}, yielding 0.16 mJ s^{-1} of blue energy.

In conclusion, the MEG ball network represents a novel and efficient platform for harvesting ocean wave energy and powering self-sustained seawater-splitting. Exhibiting a high current density (0.24 mA cm^{-2}) and low resistance (9 Ω) at a 2 Hz frequency, this self-floating network combines magnetoelastic and electromagnetic effects to generate electricity. Its robustness, waterproof nature, and high durability make it suitable for varied ocean conditions. By connecting eight MEG balls in series, we successfully increased the electric output, facilitating sustainable H_2 fuel production at a rate of 0.76×10^{-3} mL min^{-1}. This MEG ball network-based system is a significant advancement in harnessing renewable ocean wave energy for *on-site* electricity generation and H_2 production, marking a substantial contribution to the global energy supply and environmental conservation.

ASSOCIATED CONTENT

Supporting Information

The Supporting Information is available free of charge at https://pubs.acs.org/doi/10.1021/acsenergylett.4c00412.

> Experimental methods (MEG unit fabrication, MEG ball network fabrication, structural characterizations, electrical performance measurement, and electrochemical measurement), working mechanism of a MEG ball, additional data of SEM image, magnetic field variations, simulated magnetic flux density distribution, the MEG ball network output performance, and LSV curve (PDF)

AUTHOR INFORMATION

Corresponding Author

Jun Chen – *Department of Bioengineering, University of California, Los Angeles, Los Angeles, California 90095, United States*; orcid.org/0000-0002-3439-0495; Email: jun.chen@ucla.edu

Authors

Il Woo Ock – *Department of Bioengineering, University of California, Los Angeles, Los Angeles, California 90095, United States*

Yihao Zhou – *Department of Bioengineering, University of California, Los Angeles, Los Angeles, California 90095, United States*

Xun Zhao – *Department of Bioengineering, University of California, Los Angeles, Los Angeles, California 90095, United States*

Farid Manshaii – *Department of Bioengineering, University of California, Los Angeles, Los Angeles, California 90095, United States*

Complete contact information is available at: https://pubs.acs.org/10.1021/acsenergylett.4c00412

Author Contributions

[†]Il Woo Ock and Yihao Zhou contributed equally to this work.

Notes

The authors declare no competing financial interest.

ACKNOWLEDGMENTS

The authors acknowledge the Henry Samueli School of Engineering & Applied Science and the Department of Bioengineering at the University of California, Los Angeles for their startup support. J.C. acknowledges the Vernroy Makoto Watanabe Excellence in Research Award at the UCLA Samueli School of Engineering, the Office of Naval Research Young Investigator Award (Award ID: N00014-24-1-2065), NIH Grant (Award ID: R01 CA287326), the American Heart Association Innovative Project Award (Award ID: 23IPA1054908), the American Heart Association Transformational Project Award (Award ID: 23TPA1141360), the American Heart Association's Second Century Early Faculty Independence Award (Award ID: 23SCEFIA1157587), the Brain & Behavior Research Foundation Young Investigator Grant (Grant Number: 30944), and the NIH National Center for Advancing Translational Science UCLA CTSI (Grant Number: KL2TR001882). I.W.O. acknowledges the Postdoctoral Fellowship Program (Nurturing Next-generation Researchers) granted by the National Research Foundation of Korea (2021R1A6A3A14045141).

REFERENCES

(1) Tollefson, J. Blue energy. *Nature* **2014**, *508*, 302–304.

(2) Pecunia, V.; Silva, S. R. P.; Phillips, J. D.; Artegiani, E.; Romeo, A.; Shim, H.; Park, J.; Kim, J. H.; Yun, J. S.; Welch, G. C.; et al. Roadmap on energy harvesting materials. *J. Phys. Mater.* **2023**, *6*, 042501.

(3) Son, J. H.; Chung, S. H.; Cha, K.; Kim, S.; Lin, Z. H.; Hong, J.; Chung, J.; Lee, S. Ultrahigh performance, serially stackable, breeze driven triboelectric generator via ambient air ionizing channel. *Adv. Mater.* **2023**, *35*, 2300283.

(4) Heo, D.; Son, J. H.; Yong, H.; Hur, J.; Cha, K.; Kim, S.; Choi, M.; Hong, J.; Lee, S. Synergistic effect of unidirectional charge accumulation and electrostatic discharge: Simplified design approach for dramatic output enhancement of triboelectric nanogenerator. *Nano Energy* **2023**, *116*, 108793.

(5) Muetze, A.; Vining, J. G. Ocean Wave Energy Conversion - A Survey. *IEEE Ind. Applic. Soc.* **2006**, *3*, 1410–1417.

(6) Leijon, J.; Bostrom, C. Freshwater production from the motion of ocean waves - A review. *Desalination* **2018**, *435*, 161–171.

(7) Beeby, S. P.; Tudor, M. J.; White, N. M. Energy harvesting vibration sources for microsystems applications. *Meas. Sci. Technol.* **2006**, *17*, R175–R195.

(8) Viet, N. V.; Xie, X. D.; Liew, K. M.; Banthia, N.; Wang, Q. Energy harvesting from ocean waves by a floating energy harvester. *Energy* **2016**, *112*, 1219–1226.

(9) Farrok, O.; Ahmed, K.; Tahlil, A. D.; Farah, M. M.; Kiran, M. R.; Islam, M. R. Electrical Power Generation from the Oceanic Wave for Sustainable Advancement in Renewable Energy Technologies. *Sustainability* **2020**, *12*, 2178.

(10) Li, M.; Jing, X. J. A bistable X-structured electromagnetic wave energy converter with a novel mechanical-motion-rectifier: Design, analysis, and experimental tests. *Energy Convers. Manage* **2021**, *244*, 114466.

(11) Zhao, L. C.; Zou, H. X.; Wei, K. X.; Zhou, S. X.; Meng, G.; Zhang, W. M. Mechanical Intelligent Energy Harvesting: From Methodology to Applications. *Adv. Energy Mater.* **2023**, *13*, 2300557.

(12) Falcao, A. F. D. O. Wave energy utilization: A review of the technologies. *Renewable Sustainable Energy Rev.* **2010**, *14*, 899–918.

(13) Wang, Z. L.; Jiang, T.; Xu, L. Toward the blue energy dream by triboelectric nanogenerator networks. *Nano Energy* **2017**, *39*, 9−23.
(14) Scruggs, J.; Jacob, P. Harvesting Ocean Wave Energy. *Science* **2009**, *323*, 1176−1178.
(15) Wang, Z. L. Catch wave power in floating nets. *Nature* **2017**, *542*, 159−160.
(16) Leung, S. F.; Fu, H. C.; Zhang, M.; Hassan, A. H.; Jiang, T.; Salama, K. N.; Wang, Z. L.; He, J. H. Blue energy fuels: converting ocean wave energy to carbon-based liquid fuels via CO_2 reduction. *Energy Environ. Sci.* **2020**, *13*, 1300−1308.
(17) Li, S.; Jiang, J.; Zhai, N.; Liu, J.; Feng, K.; Chen, Y.; Wen, Z.; Sun, X.; Zhong, J. A half-wave rectifying triboelectric nanogenerator for self-powered water splitting towards hydrogen production. *Nano Energy* **2022**, *93*, 106870.
(18) Yang, Y.; Zhang, H.; Lin, Z. H.; Liu, Y.; Chen, J.; Lin, Z.; Zhou, Y. S.; Wong, C. P.; Wang, Z. L. A hybrid energy cell for self-powered water splitting. *Energy Environ. Sci.* **2013**, *6*, 2429−2434.
(19) Kuang, Y.; Kenney, M. J.; Meng, Y.; Hung, W. H.; Liu, Y.; Huang, J. E.; Prasanna, R.; Li, P.; Li, Y.; Wang, L.; et al. Solar-driven, highly sustained splitting of seawater into hydrogen and oxygen fuels. *Proc. Natl. Acad. Sci. U. S. A.* **2019**, *116*, 6624−6629.
(20) Yang, H.; Deng, M.; Zeng, Q.; Zhang, X.; Hu, J.; Tang, Q.; Yang, H.; Hu, C.; Xi, Y.; Wang, Z. L. Polydirectional Microvibration Energy Collection for Self-Powered Multifunctional Systems Based on Hybridized Nanogenerators. *ACS Nano* **2020**, *14*, 3328−3336.
(21) Zhai, N.; Wen, Z.; Chen, X.; Wei, A.; Sha, M.; Fu, J.; Liu, Y.; Zhong, J.; Sun, X. Blue Energy Collection toward All-Hours Self-Powered Chemical Energy Conversion. *Adv. Energy Mater.* **2020**, *10*, 2001041.
(22) Zhang, Q.; Liang, Q.; Nandakumar, D. K.; Qu, H.; Shi, Q.; Alzakia, F. I.; Tay, D. J. J.; Yang, L.; Zhang, X.; Suresh, L.; et al. Shadow enhanced self-charging power system for wave and solar energy harvesting from the ocean. *Nat. Commun.* **2021**, *12*, 616.
(23) Feng, Y.; Han, J.; Xu, M.; Liang, X.; Jiang, T.; Li, H.; Wang, Z. L. Blue Energy for Green Hydrogen Fuel: A Self-Powered Electrochemical Conversion System Driven by Triboelectric Nanogenerators. *Adv. Energy Mater.* **2022**, *12*, 2103143.
(24) Zhang, B.; Zhang, C.; Yang, O.; Yuan, W.; Liu, Y.; He, L.; Hu, Y. X.; Zhao, Z.; Zhou, L.; Wang, J.; et al. Self-Powered Seawater Electrolysis Based on a Triboelectric Nanogenerator for Hydrogen Production. *ACS Nano* **2022**, *16*, 15286−15296.
(25) Zhang, W.; He, W.; Dai, S.; Ma, F.; Lin, P.; Sun, J.; Dong, L.; Hu, C. Wave energy harvesting based on multilayer beads integrated spherical TENG with switch triggered instant discharging for self-powered hydrogen generation. *Nano Energy* **2023**, *111*, 108432.
(26) Zhou, Y.; Zhao, X.; Xu, J.; Fang, Y.; Chen, G.; Song, Y.; Li, S.; Chen, J. Giant magnetoelastic effect in soft systems for bioelectronics. *Nat. Mater.* **2021**, *20*, 1670−1676.
(27) Villari, E. Ueber die Aenderungen des magnetischen Moments, welche der Zug und das Hindurchleiten eines galvanischen Stroms in einem Stabe von Stahl oder Eisen hervorbringen. *Annu. Rev. Phys. Chem.* **1865**, *202*, 87−122.
(28) Yamaura, S.; Nakajima, T.; Satoh, T.; Ebata, T.; Furuya, Y. Magnetostriction of heavily deformed Fe-Co binary alloys prepared by forging and cold rolling. *Mater. Sci. Eng., B* **2015**, *193*, 121−129.
(29) Su, Q.; Morillo, J.; Wen, Y.; Wuttig, M. Young's modulus of amorphous Terfenol-D thin films. *J. Appl. Phys.* **1996**, *80*, 3604−3606.
(30) Datta, S.; Atulasimha, J.; Mudivarthi, C.; Flatau, A. B. Stress and magnetic field-dependent Young's modulus in single crystal iron-gallium alloys. *J. Magn. Magn. Mater.* **2010**, *322*, 2135−2144.
(31) Chen, G.; Zhou, Y.; Fang, Y.; Zhao, X.; Shen, S.; Tat, T.; Nashalian, A.; Chen, J. Wearable Ultrahigh Current Power Source Based on Giant Magnetoelastic Effect in Soft Elastomer System. *ACS Nano* **2021**, *15*, 20582−20589.
(32) Zhao, X.; Nashalian, A.; Ock, I. W.; Popoli, S.; Xu, J.; Yin, J.; Tat, T.; Libanori, A.; Chen, G.; Zhou, Y.; et al. A Soft Magnetoelastic Generator for Wind-Energy Harvesting. *Adv. Mater.* **2022**, *34*, 2204238.
(33) Ock, I. W.; Zhao, X.; Tat, T.; Xu, J.; Chen, J. Harvesting Hydropower via a Magnetoelastic Generator for Sustainable Water Splitting. *ACS Nano* **2022**, *16*, 16816−16823.
(34) Xu, J.; Tat, T.; Zhao, X.; Xiao, X.; Zhou, Y.; Yin, J.; Chen, K.; Chen, J. Spherical Magnetoelastic Generator for Multidirectional Vibration Energy Harvesting. *ACS Nano* **2023**, *17*, 3865−3872.
(35) Wu, R. Q.; Chen, L. J.; Shick, A.; Freeman, A. J. First-principles determinations of magneto-crystalline anisotropy and magneto-striction in bulk and thin-film transition metals. *J. Magn. Magn. Mater.* **1998**, *177*, 1216−1219.
(36) Tong, W.; Forster, M.; Dionigi, F.; Dresp, S.; Sadeghi Erami, R.; Strasser, P.; Cowan, A. J.; Farras, P. Electrolysis of low-grade and saline surface water. *Nat. Energy* **2020**, *5*, 367−377.
(37) Roger, I.; Shipman, M. A.; Symes, M. D. Earth-abundant catalysts for electrochemical and photoelectrochemical water splitting. *Nat. Rev. Chem.* **2017**, *1*, 0003.
(38) Dresp, S.; Dionigi, F.; Klingenhof, M.; Strasser, P. Direct Electrolytic Splitting of Seawater: Opportunities and Challenges. *ACS Energy Lett.* **2019**, *4*, 933−942.

https://doi.org/10.1021/acsenergylett.4c00412
ACS Energy Lett. 2024, 9, 1701−1709